Observation of Intermolecular Charge Transfer in a Quasi-One-Dimensional Molecular Alloy System

Xiaoming Ren*

College of Science, Nanjing University of Technology, Nanjing 210009, and Coordination Chemistry Institute & State Key Laboratory, Nanjing University, Nanjing 210093, People's Republic of China

Yunxia Sui

Centre of Modern Analysis, Nanjing University, Nanjing 210093, People's Republic of China

Guangxiang Liu

Anhui Key Laboratory of Functional Coordination Compounds, Anqing Normal College, Anqing 246011, People's Republic of China

Jingli Xie

School of Chemistry & Bio21 Institute, the University of Melbourne, Parkville, Victoria 3010, Australia

Received: January 29, 2008; Revised Manuscript Received: July 11, 2008

X-band single-crystal electron paramagnetic resonance (EPR) studies of the molecular alloy $[NO_2BzPy][Au_{0.57}Ni_{0.43}(mnt)_2]$ are presented in this paper. At room temperature, EPR spectra show both intense resonance signals (main signals) and weak satellite quartet lines. The characteristics of both intense and weak EPR signals depend on the magnetic field orientation. The main signals arise from two magnetically nonequivalent $[Ni(mnt)_2]^-$ anions, and their corresponding principal values of the g tensor are $(g_x')_1 = 2.04653$, $(g_y')_1 = 2.00096$, and $(g_z')_1 = 2.15319$ and $(g_x')_2 = 2.04520$, $(g_y')_2 = 1.99734$, and $(g_z')_2 = 2.15361$, respectively. The weak satellite lines, whose patterns strongly depend on the magnetic field direction, can be attributed to the hyperfine coupling of the electron spin with the ^{197}Au nucleus of the $[Au(mnt)_2]^-$ species. Density functional theory calculations for the spin and charge distributions of the dimer $\{[Ni(mnt)_2][Au(mnt)_2]\}^{2-}$ indicate that the hyperfine interaction of the electron spin with the ^{197}Au nuclear spins is caused, in part, by the charge transfer between the $[Ni(mnt)_2]^-$ and the $[Au(mnt)_2]^-$ species.

Introduction

Spin bistable molecular systems have recently attracted considerable attention because of their potential use in spintronic devices such as molecular switches, data storage units, and displays.[1−7] This rapidly emerging field includes the development of new spin transition systems[1,2] as well as the transition metal spin-crossover compounds. For example, a molecular system exhibiting a spin transition can be triggered by charge transfer between different magnetic centers,[8−12] charge/valence ordering in a mixed-valence compound,[13] or magneto-elastic interactions in quasi-one-dimensional (1D) antiferromagnetically coupled S = 1/2 Heisenberg or XY magnetic chains.[14]

The molecular architectures of $[M(mnt)_2]^-$ (mnt^{2-} = maleonitriledithiolate; M = Ni, Pd, or Pt), with flat molecular and extended electronic structures, are favorable for forming columnar stacks that behave as S = 1/2 magnetic chains. In our previous studies, a series of quasi-1D spin systems based on the compounds $[RBzPy][Ni(mnt)_2]$ ($[BzPy]^+$ = benzylpyridinium derivative; R represents substituent group) have been investigated, among which more than 20 compounds exhibited a spin-Peierls type transition.[10,12,15] By replacing the $[Ni(mnt)_2]^-$ monoanion with the planar $[Au(mnt)_2]^-$ anion, we obtained the diamagnetic compound $[NO_2BzPy][Au(mnt)_2]$, which is isostructural with $[NO_2BzPy][Ni(mnt)_2]$.[16] The similar molecular and crystal structure characteristics between $[NO_2BzPy][Au(mnt)_2]$ and $[NO_2BzPy][Ni(mnt)_2]$ indicated that these two compounds are ideal for preparing solid solutions of $[NO_2BzPy][Au_xNi_{1-x}(mnt)_2]$ (see Scheme 1). We further investigated the effect of nonmagnetic $[NO_2BzPy][Au(mnt)_2]$ doping in the lattice of $[NO_2BzPy][Ni(mnt)_2]$ on the spin-Peierls type transi-

SCHEME 1

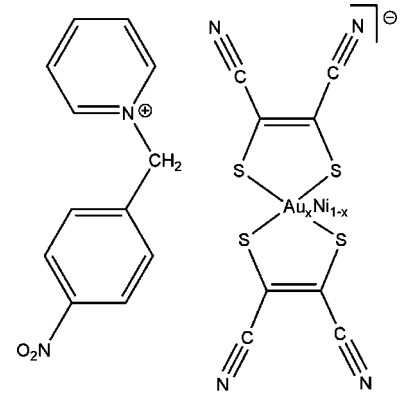

(Abbr. as $[NO_2BzPy][Au_xNi_{1-x}(mnt)_2]$)

* To whom correspondence should be addressed. Tel: +86 25-83587438. Fax: +86 25-83587438. E-mail: xmren@njut.edu.cn.

10.1021/jp8009194 CCC: $40.75
Published on Web 08/12/2008

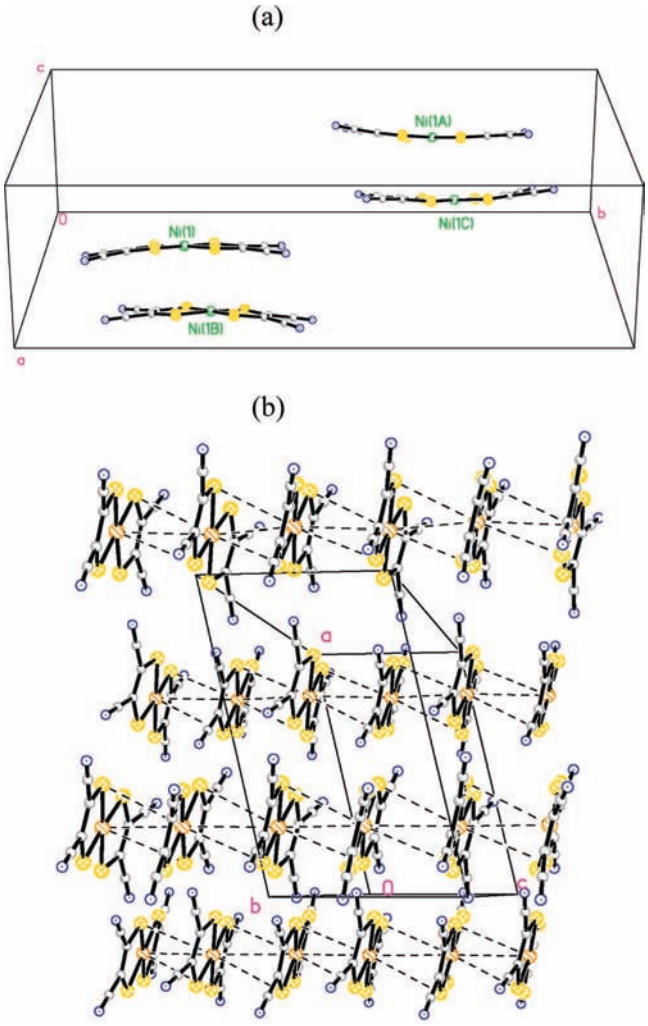

Figure 1. (a) Four anionic species related via symmetric operations in a unit cell and (b) anionic stacks projected along the *b*-axis.

tion and found that the transition is suppressed by nonmagnetic doping and collapsed at around $x > 0.27$, and in a heavier doped system, $x = 0.49$, the spin gap vanishes and a gapless phase is achieved again.[16] The magnetic behavior of $[NO_2BzPy][Au_xNi_{1-x}(mnt)_2]$ is very similar to the phenomena observed in inorganic spin-Peierls transition systems such as $CuGO_3$[17] and $TlCuCl_3$.[18] However, the transition collapsed when x values were much higher than those found in the inorganic spin-Peierls transition systems.

In this contribution, we present results of single-crystal electron paramagnetic resonance (EPR) studies for the molecular alloy $[NO_2BzPy][Au_{0.57}Ni_{0.43}(mnt)_2]$, which provides appreciable evidence of charge transfer from neighboring $[Ni(mnt)_2]^-$ to $[Au(mnt)_2]^-$ species.

Experimental Section

Single-Crystal EPR Measurements. A crystal of $[NO_2BzPy][Au_{0.57}Ni_{0.43}(mnt)_2]$[16] with dimensions 2.5 × 0.5 × 0.1 mm^3 was used for X-band EPR measurement at room temperature. An experimental orthogonal system (x, y, z) was chosen; the x-axis was along the longest edge of the crystal (corresponding to the crystallographic c-axis), the y-axis was parallel to the second longest edge of the crystal (corresponding to the crystallographic b-axis), and the z-axis was then defined using a right-handed coordinate system (see the Supporting Information, Scheme S1). The magnetic field direction was fixed while the crystal was allowed to rotate, and EPR spectra were recorded at intervals of 5° on a Bruker EMX spectrometer at room temperature.

UV−Vis-NIR Absorption Spectra. UV−vis-NIR absorption spectra in the solid state (KBr disk) and acetonitrile solution (the concentration $C \approx 5.0 \times 10^{-5}$ mol L^{-1} for each sample) were taken using a Cary 5000 UV−vis-NIR and a Lambda 35 UV/vis Spectrophotometer, respectively.

Details of Density Functional theory (DFT) Calculation. All DFT calculations were carried out with the GAUSSIAN 98 program[19] on the SGI 3800 workstation. The molecular structure of the $\{[Au(mnt)_2][Ni(mnt)_2]\}^{2-}$ dimer (nontruncated) was taken directly from X-ray crystallography data at room temperature. In our previous studies, the relationship between the magnetic coupling interaction features and the $[Ni(mnt)_2]^-$ anionic stacking patterns has been investigated theoretically by DFT, and those values obtained from calculations at the UBPW91/LANL2DZ[20] level are in good agreement with the experimental results.[21] Therefore, the single-point energy calculations for the $\{[Au(mnt)_2][Ni(mnt)_2]\}^{2-}$ dimer in this contribution were performed at the UBPW91/LANL2DZ level with convergence criterion of SCF 10^{-8}.

Results and Discussion

The crystal structure and magnetic properties of $[NO_2BzPy][Au_{0.57}Ni_{0.43}(mnt)_2]$ have been reported,[16] so the essential

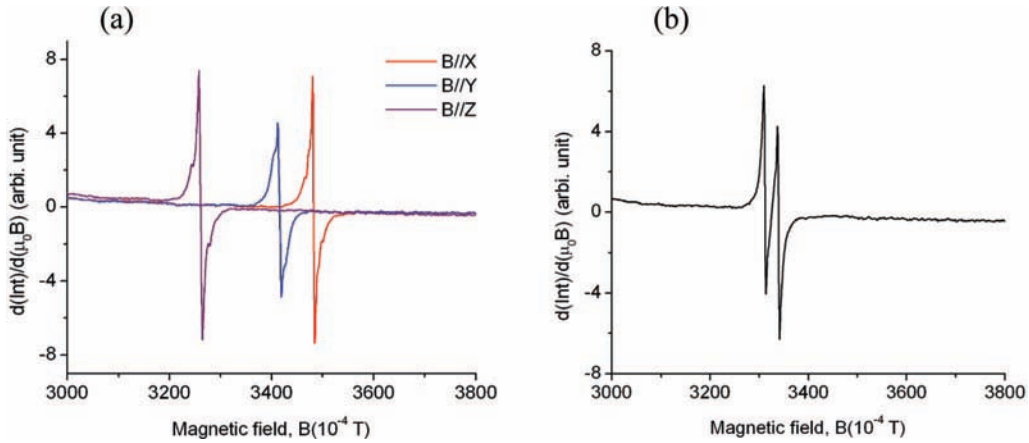

Figure 2. EPR spectra: (a) The magnetic fields are parallel to the experimental coordinate system x-, y-, and z-axes, respectively, from which main and weak EPR signals can be observed, and (b) the magnetic field lying on the yz plane and making 45° angles with the z-axis (only the main EPR signals are observed in this plot; for a detailed discussion, see the text).

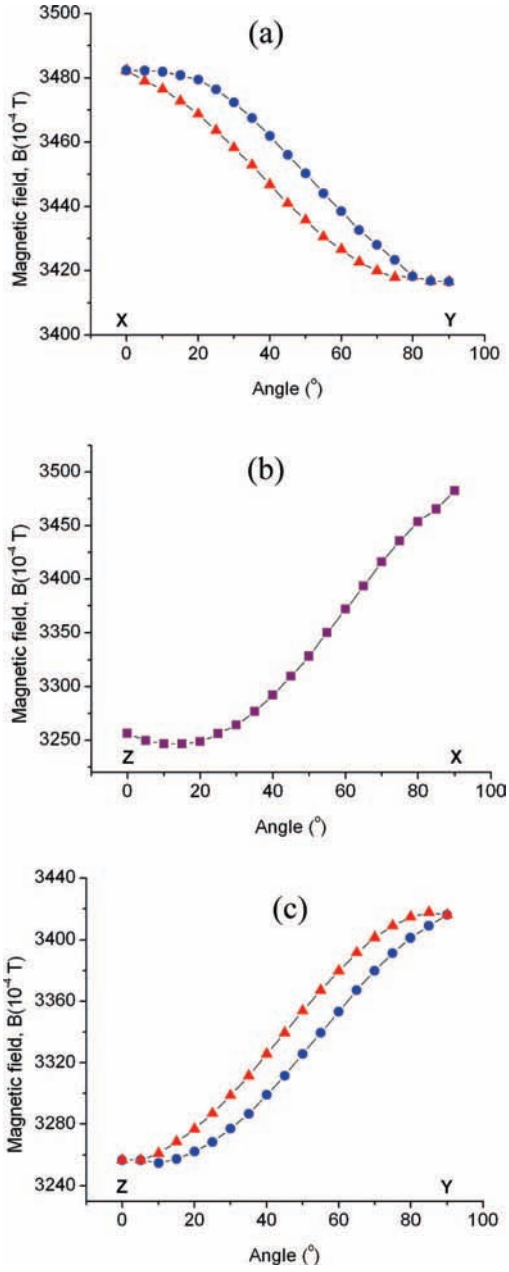

Figure 3. Angular variations of the resonance magnetic field (B_f) for the alloy compound $[NO_2BzPy][Au_{0.57}Ni_{0.43}(mnt)_2]$ (blue and red symbols represent the EPR signals from two sets of magnetically inequivalent sites, respectively).

findings are briefly summarized. At room temperature, this alloy crystallizes in the monoclinic system, $P2_1/c$ space group. The unit cell contains four identical $[Au_{0.57}Ni_{0.43}(mnt)_2]^-$ anions related by the symmetry operations of the $P2_1/c$ space group (Figure 1a). For simplicity's sake, we use the symbol Ni(1) to represent the species $[Au_{0.57}Ni_{0.43}(mnt)_2]^-$ at the general position (x, y, z) in a unit cell where Ni(1) is related to Ni(1a) by a 2-fold rotation axis (which is parallel to the b-axis), while Ni(1b) is related to Ni(1c); Ni(1) and Ni(1a) are related to Ni(1c) and Ni(1b) by an inversion center, respectively. As shown in Figure 1b, the anions form stacks along the direction of the c-axis. Within an anionic stack, the $[Ni(mnt)_2]^-$ and $[Au(mnt)_2]^-$ anions could not be distinguished from the single-crystal structure temperatures above 10 K;[16] therefore, from the viewpoint of structure, such anionic stacks should behave as a random spin-chain system.

TABLE 1: Spin-Hamiltonian Parameters for the Single Crystal of $[NO_2BzPy][Au_{0.57}Ni_{0.43}(mnt)_2]$

	principal values	the direction cosine of each principal axis (x', y', and z') with respect to the experimental coordinate system (x, y, and z)		
		x	y	z
$(g_x')_1$	2.04653	0.211660	0.976827	−0.0317557
$(g_y')_1$	2.00096	−0.953085	0.213492	0.214952
$(g_z')_1$	2.15319	0.216399	−0.0151547	0.976187
g_{av}[a]	2.06893			
$(g_x')_2$	2.04520	0.0882647	0.996086	0.00467472
$(g_y')_2$	1.99734	−0.969946	0.0848783	0.228035
$(g_z')_2$	2.15361	0.226745	−0.0246616	0.973642
g_{av}[a]	2.06538			

[a] $g_{av} = (g_x' + g_y' + g_z')/3$.

For the alloy compound $[NO_2BzPy][Au_{0.57}Ni_{0.43}(mnt)_2]$, the X-band single-crystal EPR spectra at room temperature shows intense resonance signals (main signals) from two magnetically nonequivalent molecules together with weak satellite quartet lines, and all of them are dependent on the magnetic field orientation. The representative EPR spectrum is illustrated in Figure 2. We begin by analyzing the intense EPR signals and then give a detailed discussion about the origin of the weak EPR signal. From the magnetic point of view, a unit cell can be assumed to have two magnetically nonequivalent sites in the $P2_1/c$ space group. The magnetically nonequivalent sites are related by an inversion center making them indistinguishable by EPR spectroscopy.[22] As expected for the xz plane (corresponding to the crystallographic ac) and along the crystallographic b-axis, only one resonance line was observed, since the sites are magnetically equivalent. Two lines were observed for the xy (corresponding to the crystallographic bc plane) and yz planes, which can be assigned to the anionic pairs Ni(1)−Ni(1A) and Ni(1B)−Ni(1C), respectively (Figure 1a). Although the difference between the g factors for the two magnetically nonequivalent $[Ni(mnt)_2]^-$ sites in those planes is very small, the resolution of single-crystal EPR measurements is good enough to distinguish both signals. Figure 3 shows the angular variations of the resonance magnetic field B_f where the applied magnetic field lies on the xy, xz, and yz planes, respectively. A simple diagonalization procedure for the g tensor matrix gave two sets of principal values of g, $(g_x')_1 = 2.04653$, $(g_y')_1 = 2.00096$, and $(g_z')_1 = 2.15319$ and $(g_x')_2 = 2.04520$, $(g_y')_2 = 1.99734$, and $(g_z')_2 = 2.15361$, respectively, which are close to other reported values for the $[Ni(mnt)_2]^-$ species.[23,24] The direction cosines of the g tensor principal axes (x', y', z'), with respect to three experimental axes (x, y, z), were obtained for these two sets of nonequivalent magnetic centers and are summarized in Table 1.

As shown in Figure 3, the weak EPR signals are strongly dependent on the applied magnetic field direction: The EPR signals are composed of a quartet of unequally spaced intense lines flanked on each side as the applied magnetic field, $\boldsymbol{B}$, is parallel to the x-axis, and the four satellite lines on each flank coalesce into two lines as the applied magnetic field is parallel to the y- and z-axes, respectively; the weak satellite lines disappear as $\boldsymbol{B}$ lies on the yz plane and makes a 45° angle with the z-axis.

For the anionic $[Ni(mnt)_2]^-$ species, the hyperfine splitting of EPR signal could be caused by the interactions between the unpaired electron and the magnetic nuclei such as ^{61}Ni (natural abundance = 1.14% and I = 3/2), ^{33}S (natural abundance = 0.74% and I = 3/2), ^{13}C (natural abundance = 1.10% and I =

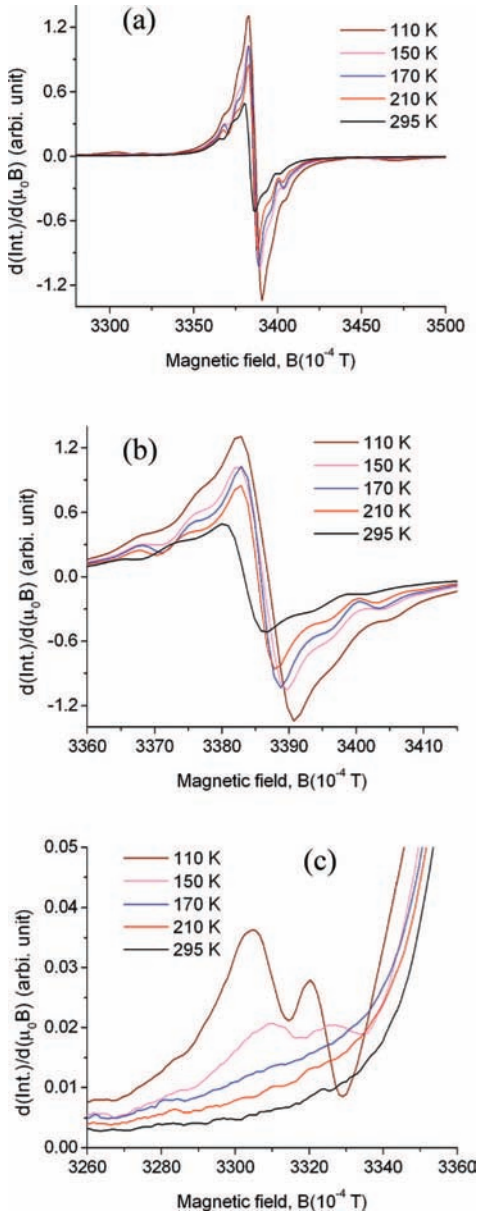

Figure 4. (a) Temperature-dependent EPR spectra measured as the magnetic fields being parallel to the experimental coordinate system *x*-axis (two new satellite lines appear on each side of the main EPR signal when the temperature is lower than 150 K; (b and c) enlarged plots.

1/2), and ^{14}N (natural abundance = 99.635% and $I = 1$). However, hyperfine interactions between an unpaired electron and the magnetic nuclei ^{61}Ni, as well as ^{33}S, are usually irresolvable because of their small splitting and lower natural abundance in $[Ni(mnt)_2]^-$ species,[24] and the hyperfine splitting patterns for ^{13}C and ^{14}N do not agree with the experimental spectra. Therefore, the possibility of the weak EPR signals resulting from the $[Ni(mnt)_2]^-$ species is ruled out. On the other hand, the characteristic spectrum for the weak EPR signals (for instance, the hyperfine splitting pattern is strongly dependent on the applied magnetic field orientation) is very similar to the EPR spectrum of $[Au(mnt)_2]^{2-}$ species, which has been observed in several magnetically dilute single crystals. So, such hyperfine splitting arises from the unpaired electron spin interactions with magnetic nuclear ^{197}Au spins (natural abundance = 100% and $I = 3/2$).[25]

For the $[Au(mnt)_2]^{2-}$ anion, the electron spin is 1/2. If the hyperfine coupling interaction between the unpaired electron spin and the ^{197}Au nuclear spin, as well as the quadrupole moment interaction of the ^{197}Au nucleus, are taken into account, then the spin Hamiltonian for such a system can be expressed by eq 1.

$$H_{sp} = \beta_e SgB - g_N \beta_N BI + \mathrm{SAI} + \mathrm{IPI} \quad (1)$$

In eq 1, the first two terms stand for the Zeeman interactions of the unpaired electron and ^{197}Au nucleus, respectively, the third term represents the hyperfine interaction between the electron spin and the ^{197}Au nucleus spins, and the last term stands for the quadrupole interaction of the ^{197}Au nucleus. Because of the fact that the ^{197}Au nucleus possesses a rather small magnetic moment as compared to its large quadrupole moment, the magnitude of the ^{197}Au hyperfine (the term SAI) and quadrupole (the term IPI) interactions are compatible. This situation leads to (i) a significant disturbance of the equidistance between the "allowed" four ^{197}Au hyperfine lines and (ii) the occurrence of up to eight "forbidden" hyperfine transitions with partially remarkable intensities depending on the magnetic direction. As a consequence, the $[Au(mnt)_2]^{2-}$ species usually shows a complicated EPR spectrum (for example, the spectrum has a large temperature dependence of the *g* tensor, the isotropic hyperfine coupling, and the quadrupole tensor as well as the deviation of the principal axis system of the *g* tensor from that of the quadrupole tensor and its temperature dependence).[25] We tried unsuccessfully to fit the spectrum and obtain the corresponding spin-Hamiltonian parameters of the *g* tensor, *A* tensor, and *P* tensor.

It was interesting to explore how the ^{197}Au nucleus spins affected the splitting of the EPR signal, spin polarization, and charge transfer. To get an insightful understanding about this issue, we performed both microwave power dependency (the power was changed from 1.25 to 20 mW, and both receiver gain and modulation amplitudes were kept the same values) and variable temperature EPR spectroscopy measurements (in the temperature range of 295−110 K). We found that the relative intensity between weak and main EPR signals is independent of the microwave power, whereas obvious increases occur with a reduction in temperature, as demonstrated in Figure 4; two new satellite lines appear on each flank of the main EPR signal. This finding, regarding the link between the relative intensity of the weak and the main EPR signals and its independence on microwave power, excludes the mechanism that the weak signals originate from the microwave-assisted electron hopping from the $[Ni(mnt)_2]^-$ anion to the $[Au(mnt)_2]^-$ anion. On the other hand, the conjugated oligomers and polymers are known to transport charge via a thermally activated hopping type mechanism.[26] If this kind of electron hopping mechanism occurs within an anionic stack in the alloy complex, the intensity for the weak EPR signals should decrease as the sample cools, while the observation that the weak EPR signal intensity increases with a reduction in temperature rules out the thermally activated hopping type mechanism. Furthermore, we calculated the charge and spin distributions for the dimer $\{[Ni(mnt)_2][Au(mnt)_2]\}^{2-}$ using a DFT theoretical framework at the UBPW91/LanL2DZ level. As mentioned above, the asymmetric unit contains one $[Au_{0.57}Ni_{0.43}(mnt)_2]^-$ anion, which forms regular stacks along the direction of *c*-axis. From the crystal structure, there is only one kind of anionic dimer within an anionic stack; therefore, the calculations for charge and spin distributions were performed on the $\{[Ni(mnt)_2][Au(mnt)_2]\}^{2-}$ dimer. The calculated spin and charge distributions are demonstrated in Figure 5a,b, which disclosed that there is small amount of charge transfer (CT) from the $[Ni(mnt)_2]$ species to the $[Au(mnt)_2]$ species ($[Ni(mnt)_2]^{-1+\delta}$ and $[Au(mnt)_2]^{-1-\delta}$; $\delta = 0.04943$ at room

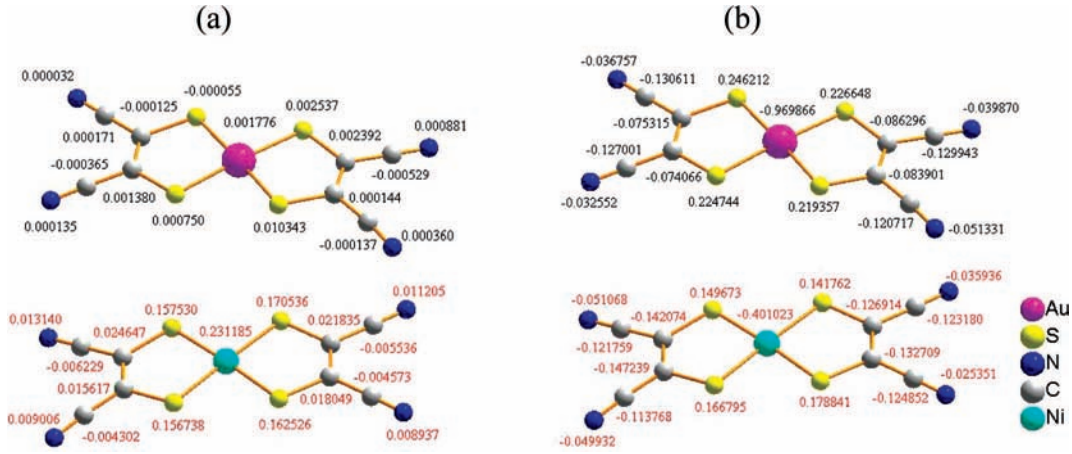

Figure 5. (a) Spin density distributions (the total α spin value is 0.01969 for the $[Au(mnt)_2]$ species and 0.98031 for the $[Ni(mnt)_2]$ species, respectively) and (b) the charge density distributions for the dimer of $\{[Ni(mnt)_2][Au(mnt)_2]\}^{2-}$ calculated by DFT at the UBPW91/LanL2DZ level.

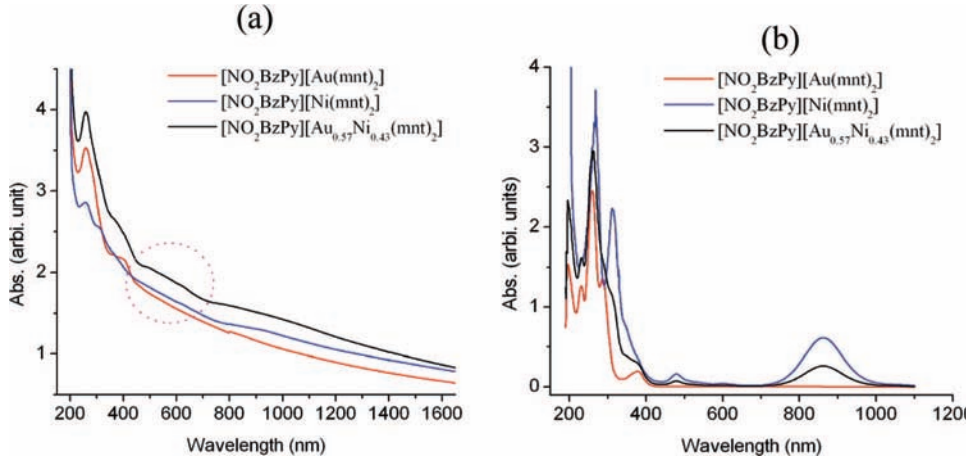

Figure 6. UV−vis-NIR spectra in (a) solid state and (b) acetonitrile solution for $[NO_2BzPy][Au(mnt)_2]$, $[NO_2BzPy][Ni(mnt)_2]$, and $[NO_2BzPy][Au_{0.57}Ni_{0.43}(mnt)_2]$.

temperature) through intermolecular π-orbital overlap. Although $\pi-\pi$ type CT phenomena have been well-known,[27] such as the intermolecular charge transfer via π orbital interaction occurs between both neutral π type electron donor and acceptor, [28] between neutral π type electron donor and cationic π type electron acceptor,[29] as well as between π type anion and cation, [30] to the best of our knowledge, it is rare that the charge transfer occurs between two anionic species; larger spin density distributions are found on Ni atom (∼0.231) and four S atoms (the values range from 0.157 to 0.170) in the $[Ni(mnt)_2]^-$ moiety, indicating the existence of a strong delocalization effect from the metal Ni atom to ligands, and the total spin population on the $[NiS_4]$ core is calculated to be about 0.872, which is close to the results in the literature; [21,31] a weak spin polarization effect (the signs of spin densities of the neighboring atoms are alternatively aligned) is observed in the mnt^{2-} ligands of $[Ni(mnt)_2]^-$ species, which is consistent with the previous results[21] but not between $[Ni(mnt)_2]^-$ and $[Au(mnt)_2]^-$ species. This may be a result of a charge transfer mechanism leading to the hyperfine coupling interaction of the unpaired electron spin with the ^{197}Au nuclear spin.

To get more evidence for intermolecular charge transfer, the UV−vis-NIR spectra of pure $[NO_2BzPy][Au(mnt)_2]$ and $[NO_2BzPy][Ni(mnt)_2]$ complexes, as well as the molecular alloy complex $[NO_2BzPy][Au_{0.57}Ni_{0.43}(mnt)_2]$ in solids and acetonitrile solutions, were measured, and the plots are shown respectively in Figure 6a,b. In solid-state UV−vis-NIR spectra, two parent complexes $[NO_2BzPy][Au(mnt)_2]$ and $[NO_2BzPy][Ni(mnt)_2]$ do not show obvious absorbance (see the area marked by a circle in Figure 6a), while the alloy complex $[NO_2BzPy][Au_{0.57}Ni_{0.43}(mnt)_2]$ exhibits a weak and broad absorption band in the range of 450−720 nm. This new absorbance probably originates from the intermolecular charge transfer between the neighboring $[Ni(mnt)_2]^-$ and $[Au(mnt)_2]^-$ anions. In a dilute acetonitrile solution (the concentration $C \approx 5 \times 10^{-5}$ mol L^{-1} for each complex), with respect to the spectra of two parent complexes $[NO_2BzPy][Au(mnt)_2]$ and $[NO_2BzPy][Ni(mnt)_2]$, no new visible absorption band is observed in the range of 450−720 nm. This situation is understandable because the charge transfer between neighboring species through $\pi\cdots\pi$ orbital interaction is spatially dependent.[32] The Coulomb repulsive interactions between $[Ni(mnt)_2]^-$ and $[Au(mnt)_2]^-$ anions will cause them to separate with each other in solution, and in this case, the efficient overlap for π-orbitals between $[Ni(mnt)_2]^-$ and $[Au(mnt)_2]^-$ anions is unavailable, which might be the reason for no obvious CT band for the alloy system in solution.

Conclusion

We performed the single-crystal EPR measurements for a quasi-1D molecular alloy system, $[NO_2BzPy][Au_{0.57}Ni_{0.43}(mnt)_2]$, from which two kinds of EPR signals were observed. The main EPR signals without hyperfine splitting arise from a spin present in the $[Ni(mnt)_2]^-$ species, whereas the weak EPR

signals with 4-fold unequally spaced hyperfine splitting lines come from the hyperfine interaction between the unpaired electron spin and the ^{197}Au nuclear spin. DFT calculations for spin and charge distributions in a dimer of $\{[Ni(mnt)_2][Au(mnt)_2]\}^{2-}$ showed that the hyperfine coupling interaction mechanism between unpaired electron spin and ^{197}Au nucleus spins is caused by a small amount of intermolecular charge transfer from the $[Ni(mnt)_2]^-$ to the $[Au(mnt)_2]^-$ species. Additionally, evidence for intermolecular charge transfer is further given by the UV−vis-NIR spectra of $[NO_2BzPy][Au(mnt)_2]$, $[NO_2BzPy][Ni(mnt)_2]$, and $[NO_2BzPy][Au_{0.57}Ni_{0.43}(mnt)_2]$ in solid state; a new absorption band in the 450−720 nm region appears for $[NO_2BzPy][Au_{0.57}Ni_{0.43}(mnt)_2]$ but does not come into sight in the UV−vis-NIR spectra of $[NO_2BzPy][Au(mnt)_2]$ and $[NO_2BzPy][Ni(mnt)_2]$.

Acknowledgment. We thank the Science and Technology Department of Jiangsu Province, People's Republic of China for financial support (Grant BK2007184). J.X. thanks Brett M. Paterson for reading the manuscript and also acknowledges the financial support of the Australian Research Council. X.M.R. greatly appreciates Dr. Nathan J. Silvernail for reading the manuscript and helpful discussion.

Supporting Information Available: PDF file containing a schematic describing the choice of the experimental orthogonal system (*x*, *y*, *z*) in the single-crystal EPR measurement. This material is available free of charge via the Internet at http://pubs.acs.org.

References and Notes

(1) Itkis, M. E.; Chi, X.; Cordes, A. W.; Haddon, R. C. *Science* **2002**, *296*, 1443.

(2) Fujita, W.; Awaga, K. *Science* **1999**, *286*, 261.

(3) Kahn, O.; Martinez, C. J. *Science* **1998**, *279*, 44.

(4) Garcia, Y.; Moscovici, J.; Michalowicz, A.; Ksenofontov, V.; Levchenko, G.; Bravic, G.; Chasseau, D.; Gütlich, P. *Chem. Eur. J.* **2002**, *8*, 4992.

(5) Gutlich, P.; Garcia, Y.; Woike, T. *Coord. Chem. Rev.* **2001**, *219*, 839.

(6) (a) Leita, B. A.; Neville, S. M.; Halder, G. J.; Moubaraki, B.; Kepert, C. J.; Létard, J.-F.; Murray, K. S. *Inorg. Chem.* **2007**, *46*, 8784. (b) Klokishner, S.; Linares, J. *J. Phys. Chem. C* **2007**, *111*, 10644. (c) Bousseksou, A.; Molnar, G.; Matouzenko, G. *Eur. J. Inorg. Chem.* **2004**, *22*, 4353.

(7) Letard, J. F.; Guionneau, P.; Goux-Capes, L. *Top. Curr. Chem.* **2004**, *235*, 221.

(8) (a) Park, J.-H.; Frye, F.; Anderson, N. E.; Pajerowski, D. M.; Huh, Y. D.; Talham, D. R.; Meisel, M. W. *J. Magn. Magn. Mater.* **2007**, *310*, 1458. (b) Papanikolaou, D.; Kosaka, W.; Margadonna, S.; Kagi, H.; Ohkoshi, S.; Prassides, K. *J. Phys. Chem. C* **2007**, *111*, 8086. (c) Papanikolaou, D.; Margadonna, S.; Kosaka, W.; Ohkoshi, S.; Brunelli, M.; Prassides, K. *J. Am. Chem. Soc.* **2006**, *128*, 8358. (d) Umezono, Y.; Fujita, W.; Awaga, K. *J. Am. Chem. Soc.* **2006**, *128*, 1084. (e) Ohkoshi, S.; Matsuda, T.; Tokoro, H.; Hashimoto, K. *Chem. Mater.* **2005**, *17*, 81. (f) Shimamoto, N.; Ohkoshi, S.; Sato, O.; Hashimoto, K. *Inorg. Chem.* **2002**, *41*, 678.

(9) Berlinguette, C. P.; Dragulescu-Andrasi, A.; Sieber, A.; Galán-Mascarós, J. R.; Güdel, H.; Achim, C.; Dunbar, K. R. *J. Am. Chem. Soc.* **2004**, *126*, 6222.

(10) Xie, J. L.; Ren, X. M.; He, C.; Song, Y.; Meng, Q. J.; Kremer, R. K.; Yao, Y. G. *Chem. Phys. Lett.* **2003**, *369*, 41.

(11) Ren, X. M.; Nishihara, S.; Akutagawa, T.; Noro, S.; Nakamura, T.; Fujita, W.; Awaga, K.; Ni, Z. P.; Xie, J. L.; Meng, Q. J.; Kremer, R. K. *Dalton Trans.* **2006**, 1988.

(12) Ni, C. L.; Dang, D. B.; Song, Y.; Gao, S.; Li, Y. Z.; Ni, Z. P.; Tian, Z. F.; Wen, L. L.; Meng, Q. J. *Chem. Phys. Lett.* **2004**, *396*, 353.

(13) Yamashita, M.; Kawakami, D.; Matsunaga, S.; Nakayama, Y.; Sasaki, M.; Takaishi, S.; Iwahori, F.; Miyasaka, H.; Sugiura, K.; Wada, Y.; Miyamae, H.; Matsuzaki, H.; Okamoto, H.; Tanaka, H.; Marumoto, K.; Kuroda, S. *Angew. Chem., Int. Ed.* **2004**, *43*, 4763.

(14) (a) Jeannin, O.; Clérac, R.; Fourmigué, M. *J. Am. Chem. Soc.* **2006**, *128*, 14649. (b) Willett, R. D.; Garcŕa, C. J. G.; Ramakrishna, B. L.; Twamley, B. *Polyhedron* **2005**, *24*, 2232.

(15) (a) Ren, X. M.; Meng, Q. J.; Song, Y.; Lu, C. S.; Hu, C. J.; Chen, X. Y. *Inorg. Chem.* **2002**, *41*, 5686. (b) Ren, X. M.; Okudera, H.; Kremer, R. K.; Song, Y.; He, C.; Meng, Q. J.; Wu, P. H. *Inorg. Chem.* **2004**, *43*, 2569. (c) Dang, D. B.; Ni, C. L.; Bai, Y.; Tian, Z. F.; Ni, Z. P.; Wen, L. L.; Meng, Q. J.; Gao, S. *Chem. Lett.* **2005**, *34*, 680. (d) Ren, X. M.; Akutagawa, T.; Nishihara, S.; Nakamura, T.; Fujita, W.; Awaga, K. *J. Phys. Chem. B* **2005**, *109*, 16610. (e) Ni, C. L.; Yu, L. L.; Yang, L. M. *Inorg. Chim. Acta* **2006**, *359*, 1383. (f) Ni, C. L.; Zhou, J. R.; Tian, Z. F.; Ni, Z. P.; Li, Y. Z.; Meng, Q. J. *Inorg. Chem. Commun.* **2007**, *10*, 880. (g) Tian, Z. F.; Ren, X. M.; Li, Y. Z.; Song, Y.; Meng, Q. J. *Inorg. Chem.* **2007**, *46*, 8102.

(16) Ren, X. M.; Akutagawa, T.; Noro, S.; Nishihara, S.; Nakamura, T.; Yoshida, Y.; Inoue, K. *J. Phys. Chem. B* **2006**, *110*, 7671.

(17) (a) Hase, M.; Terasaki, I.; Sasago, Y.; Uchinokura, K. *Phys. Rev. Lett.* **1993**, *71*, 4059. (b) Oseroff, S. B.; Cheong, S. W.; Aktas, B.; Hundley, M. F.; Fisk, Z.; Rupp, L. W. *Phys* **1995**, *74*, 1450. (c) Masuda, T.; Fujioka, A.; Uchiyama, Y.; Tsukada, I.; Uchinokura, K. *Phys. Rev. Lett.* **1998**, *80*, 4566.

(18) Oosawa, A.; Ono, T.; Tanaka, H. *Phys. Rev. B* **2002**, *66*, 020405.

(19) Frisch, M. J.; Trucks, G. W.; Schlegel, H. B.; Scuseria, G. E.; Robb, M. A.; Cheeseman, J. R.; Zakrzewski, V. G.; Montgomery, J. A.; Stratmann, R. E., Jr.; Burant, J. C.; Dapprich, S.; Millam, J. M.; Daniels, A. D.; Kudin, K. N.; Strain, M. C.; Farkas, O.; Tomasi, J.; Barone, V.; Cossi, M.; Cammi, R.; Mennucci, B.; Pomelli, C.; Adamo, C.; Clifford, S.; Ochterski, J.; Petersson, G. A.; Ayala, P. Y.; Cui, Q.; Morokuma, K.; Salvador, P.; Dannenberg, J. J.; Malick, D. K.; Rabuck, A. D.; Raghavachari, K.; Foresman, J. B.; Cioslowski, J.; Ortiz, J. V.; Baboul, A. G.; Stefanov, B. B.; Liu, G.; Liashenko, A.; Piskorz, P.; Komaromi, I.; Gomperts, R.; Martin, R. L.; Fox, D. J.; Keith, T.; Al-Laham, M. A.; Peng, C. Y.; Nanayakkara, A.; Challacombe, M.; Gill, P. M. W.; Johnson, B.; Chen, W.; Wong, M. W.; Andres, J. L.; Gonzalez, C.; Head-Gordon, M.; Replogle, E. S.; Pople, J. A. *Gaussian 98*, Revision A.11; Gaussian, Inc.: Pittsburgh PA, 2001.

(20) (a) Becke, A. D. *Phys. Rev. A* **1988**, *38*, 3098. (b) Perdew, J. P.; Burke, K.; Wang, K. *Phys. Rev. B* **1996**, *54*, 16533. (c) Dunning, T. H., Jr.; Hay, P. J. In *Methods of Electronic Structure Theory*; Schaefer, H. F., III, Ed.; Plenum Press: New York, 1976; Vol. 3, p 1. (d) Hay, P. J.; Wadt, W. R. *J. Chem. Phys.* **1985**, *82*, 270. (e) Wadt, W. R.; Hay, P. J. *J. Chem. Phys.* **1985**, *82*, 284. (f) Hay, P. J.; Wadt, W. R. *J. Chem. Phys.* **1985**, *82*, 299.

(21) Ni, Z. P.; Ren, X. M.; Ma, J.; Xie, J. L.; Ni, C. L.; Chen, Z. D.; Meng, Q. J. *J. Am. Chem. Soc.* **2005**, *127*, 14330.

(22) (a) Bencini, A.; Gatteschi, D. *EPR of Exchange Coupled Systems*; Springer-Verlag: Berlin, Heildelberg, Germany, 1990. (b) Tamayo, A.; Casabó, J.; Escriche, L.; González, P.; Lodeiro, C.; Rizzi, A. C.; Brondino, C. D.; Passeggi, M. C. G.; Kivekäs, R.; Sillanpää, R. *Inorg. Chem.* **2007**, *46*, 5665.

(23) (a) Maki, A. H.; Edelstein, N.; Davison, A.; Holm, R. H. *J. Am. Chem. Soc.* **1964**, *86*, 4580. (b) Stein, M.; van Lenthe, E.; Baerends, E. J.; Lubitz, W. *J. Phys. Chem. A* **2001**, *105*, 416.

(24) Kirmse, R.; Stach, J.; Dietzsch, W.; Steimeche, G.; Hoyer, E. *Inorg. Chem.* **1980**, *19*, 2679.

(25) (a) Ihlo, L.; Böttcher, R.; Olk, R.-M.; Kirmse, R. *Inorg. Chim. Acta* **1998**, *281*, 160. (b) Schlupp, R. L.; Maki, A. H. *Inorg. Chem.* **1974**, *13*, 44.

(26) (a) Epstein, A. J.; Lee, W. P.; Prigodin, V. N. *Synth. Met.* **2001**, *117*, 9. (b) Reedijk, J. A.; Martens, H. C. F.; van Bohemen, S. M. C.; Hilt, O.; Brom, H. B.; Michels, M. A. J. *Synth. Met.* **1999**, *101*, 475.

(27) Sakurai, H.; Kira, M.; Uchida, T. *J. Am. Chem. Soc.* **1973**, *95*, 6826.

(28) Kalimuthu, P.; Sivanesan, A.; John, S. A. *J. Phys. Chem. A* **2007**, *111*, 12086.

(29) Imai, Y.; Kido, S.; Kamon, K.; Kinuta, T.; Sato, T.; Tajima, N.; Kuroda, R.; Matsubara, Y. *Org. Lett.* **2007**, *9*, 5047.

(30) Uno, B.; Okumura, N.; Seto, K. *J. Phys. Chem. A* **2000**, *104*, 3064.

(31) Huyett, J. E.; Choudhury, S. B.; Eichhorn, D. M.; Bryngelson, P. A.; Maroney, M. J.; Hoffman, B. M. *Inorg. Chem.* **1998**, *37*, 1361.

(32) Hutchison, G. R.; Ratner, M. A.; Marks, T. J. *J. Am. Chem. Soc.* **2005**, *127*, 16866.

JP8009194